2018

AN INTER-WATERSHED COMPARISON STUDY OF BEDROCK CONTROLS ON SHALLOW SUBSURFACE FLOW AND STREAMFLOW RESPONSE

Robert Livesay

AN INTER-WATERSHED COMPARISON STUDY OF BEDROCK CONTROLS ON SHALLOW SUBSURFACE FLOW AND STREAMFLOW RESPONSE

By

Robert Michael Livesay

B.S. Honors, University Scholar, International Field Geosciences, University of Montana, Missoula, Montana, 2013

Thesis

presented in partial fulfillment of the requirements
for the degree of

Master of Science
in Forestry (Hydrology)

The University of Montana
Missoula, MT

Official Graduation Date (June 2018)

Approved by:

Scott Whittenburg, Dean of The Graduate School
Graduate School

Dr. Kelsey Jencso, Chair
Department of Forest Management

Dr. W. Payton Gardner, Co-Chair
Department of Geosciences

Dr. Benjamin Colman
Department of Ecosystem and Conservation Science

Livesay, Robert, M.S., June 2018 **Forestry**

AN INTER-WATERSHED COMPARISON STUDY OF BEDROCK CONTROLS ON SHALLOW SUBSURFACE FLOW AND STREAMFLOW RESPONSE

Chairperson: Dr. Kelsey Jencso

Co-Chairperson: Dr. W. Payton Gardner

Bedrock controls on watershed response have been actively studied in recent years, however, most conclusions are based on surface water analysis leaving unresolved questions about the nature of bedrock flow paths and ultimately their control on watershed response. In this study, we investigated bedrock controls on watershed response by simultaneously monitoring the hydrology of two adjacent watersheds underlain by dissimilar geologic formations (monzonite vs. meta-sandstone) and by characterizing subsurface conditions through bedrock drilling and fracture mapping. We hypothesized, when soils saturate, the underlying bedrock geology may influence the partitioning of shallow subsurface flow (SSF) between soil and bedrock flow paths, resulting in a divergence in hillslope runoff response between each watershed. We found SSF occurred for longer periods and at greater magnitudes in the monzonite watershed relative to the meta-sandstone watershed. Furthermore, hillslopes underlain by monzonite bedrock drained more rapidly compared to the hillslopes underlain by meta-sandstone bedrock. Paired hydrometric observations of soil and bedrock flow systems linked hillslope discharge to bedrock exfiltration at the slope base. The bedrock driven control on hillslope discharge promoted a stark divergence in the streamflow response between each watershed. These findings provide strong evidence supporting a bottom up view of watershed function, where bedrock flows systems are a fundamental control on the hydrologic response of hillslopes and stream networks. Conclusions from this study bolster the need to further investigate how differences in bedrock properties across mountainous watersheds will influence the resilience of headwater basins in the face of climate change.

1.0. Introduction

The capacity of headwater basins to accumulate, store and distribute water is a fundamental part of the watershed hydrologic system (Vivirolli et al., 2003). Headwater basins supply base flow to river ecosystems and are the predominant source of recharge to semi-arid alluvial basin aquifers (Wilson and Guan, 2004). Hydrologists have shown that runoff generation in headwater catchments can be extremely variable over space and in time (Voeckler et al., 2014; Penna et al., 2014). A common theme in catchment hydrology is understanding how landscape features organize runoff generation processes across catchments (Dunne and Black, 1970; Grayson et al., 1997; Brown et al., 1999; Penna et al., 2014). However, to simplify boundary conditions some research has considered underlying bedrock to be nearly impermeable relative to overlaying soils (e.g. Weyman 1973), thus ignoring the connection between bedrock flow systems and the more well characterized shallow subsurface flow systems. While the role of bedrock flow systems in hillslope runoff generation may be limited in some instances (e.g. Gabrielli et al., 2012), recent studies (Uchida et al., 2003; Kosugi et al., 2008; Masaoka et al., 2016) have revealed bedrock flow paths contribute to hillslope runoff and ultimately streamflow (Haria and Shand, 2004). This study examined the influence of bedrock geology on runoff generation processes by studying the hydrologic response of two adjacent watersheds underlain by different lithologies. We identified the major drivers of watershed response and made insight into what hillslope parameters governed the partitioning of water between soil and bedrock and ultimately, how bedrock properties influenced the streamflow response.

In mountain landscapes, hillslopes make up the majority of watershed catchment area and are considered fundamental units of the hydrologic landscape (Graham et al., 2010 a). Hillslopes are typically located on moderate to steep grades and have shallow soils underlain by less-permeable variably weathered bedrock (Rempe and Dietrich, 2014; Jencso et al., 2009). Under these conditions, shallow subsurface flow (SSF) may occur when rain or meltwater infiltrates in excess of soil field capacity and becomes perched above a confining basal layer (Weymen, 1973; Smith et al., 2014). Transmissivity feedbacks driven by layers of changing hydraulic conductivity in the subsurface promote development of SSF (Kendall et al., 1999) and are in part controlled by seasonal precipitation inputs (Western et al., 1999),

hillslope curvature (Beven and Kirkby, 1979; Burt and Butcher, 1985) and soil properties (Weiler et al., 2005). Furthermore, gradients in orographic precipitation (Jiang, 2003) and differences in solar radiation loading on contrasting slope faces (Oliphant et al., 2003) can create heterogeneous soil moisture conditions that can influence patterns of SSF. Once SSF is initiated, the topographic configuration of a hillslope plays an important role in the routing of SSF downslope. Topographic metrics such as the Topographic Wetness Index (TWI; Beven and Kirkby, 1979) are useful to describe relative hydrologic conditions of a given site in a landscape (*Sørensen* and Seibert 2007) because its derivation approximates upslope subsurface storage and the local hydraulic gradient.

During periods of high wetness, saturated hillslope soils may become hydrologically connected to riparian areas resulting in significant quantities of water transported to adjacent riparian zones and stream networks (Jencso et al., 2009). McGlynn and McDonnell (2003) reported hillslope contribution to total catchment runoff ranged from 2-55% and was dependent upon antecedent moisture conditions and the degree of upslope to stream hydrologic connectivity. More recent investigations have moved towards a unifying framework describing the influence of catchment characteristics (e.g. topography) on SSF development and streamflow generation (Penna et al., 2014). Jencso and others (2009) demonstrated larger catchment drainage areas exhibited longer durations of hydrologic connectivity between hillslope-riparian-stream wells. Catchment areas with more-permeable geology had a reduction in soil hydrologic connection to adjacent riparian zones (Jensco and McGlynn 2011).

This concept was later tested utilizing a water balance approach (Bergstrom et al., 2016). Bergstrom and others (2016) reported watershed contributing areas underlain by more permeable bedrock (sandstone) yielded less water per unit area across flow states relative to reaches with less permeable bedrock (granite gneiss). Similar to Bergstrom and others (2016), Gardner and others (2010) observed watersheds underlain by Yellowstone quaternary volcanics had slower streamflow recession and lower maximum to minimum flow ratios compared to watersheds underlain by older less permeable bedrock. While both studies demonstrate bedrock permeability as a control on streamflow, their observations were based on surface water chemistry and of the stream water balance, leaving unresolved questions about the subsurface mechanisms which lead to these observations.

More recent hillslope scale studies are beginning to investigate these subsurface mechanisms which link the impact of topography, lithology and bedrock structure on the connection between soil and bedrock flow systems. Gabrielli and others (2012), used a rotary core drill to map bedrock structure at two hillslopes in New Zealand and Oregon. They measured a bedrock water table that responded rapidly to storm events and suggest a direct connection between hillslope process and bedrock flow systems. Modelling efforts by Appels and others (2015), demonstrated that zones of high flow accumulation, bedrock fractures and zones of increased subsurface saturation may act as potential hotspot for flow between soil and bedrock systems. These studies suggest a direct connection between soil and bedrock flow systems. However, they have provided little insight into how lithological driven subsurface properties may influence SSF dynamics (height, duration) across hillslopes and watersheds.

To some degree the properties of bedrock underlying hillslopes govern the flux of water between bedrock and soil layers, thus, influencing SSF development in soils (Tromp-van Meerveld et al., 2007 and Graham et al., 2010). While recent work has correlated catchment geology with differences in streamflow response and stream water age (Bergstrom et al., 2016; Gardner et al., 2010; Hale et al., 2016b), their findings do not relate observations of streamflow to upland runoff generation from SSF. In this paper, we hypothesize when soils saturate, the underlying bedrock geology may influence the partitioning of soil water between shallow and deep flow paths, resulting in differences in runoff response in each watershed. Furthermore, we did not solely focus on lithological differences, we also characterized the topographic gradients, soils properties and atmospheric demand in each watershed and examined their relative role in hillslope runoff generation. This watershed comparison approach identified hierarchical features which influenced SSF dynamics and the resulting stream runoff response in a semi-arid mountain environment and answered the following questions:

1.1. Questions

1) How does bedrock geology influence the hydrologic response of a watershed?

2) What are the dominant controls on the partitioning of water between soil and bedrock flow systems?

2.0. Site description

2.1. General Description

The Lubrecht Experimental Forest (latitude: 46°89' N, longitude 113° 45'W) is located in the Garnet Mountain Range of Western Montana (fig. 1b)**.** This research site is located in the northeast region of the experimental forest and consists of two adjacent watersheds; Cap Wallace watershed (CW; 6.2 km²) and North Fork Elk Creek watershed (NFEC; 18.6 km²) (fig. 1a). The two watersheds are separated by an east-west trending ridgeline and both have perennial streams which feed Elk Creek, a tributary to the Blackfoot River. General climatic conditions for the research site are considered semi-arid (i.e. hot dry summers and cold snowy winters with ~ 500 mm of annual precipitation) (Hoylman et al., 2018).

2.1. Climate and vegetation

Historic meteorological conditions at the research site have been recorded from 1967-present at the Lubrecht Flume (#604) and North Fork Elk Creek (#657) snow survey and telemetry stations (SNOTEL) (fig 1.a). Mean annual temperature and precipitation for these two stations are 4.22°C with 514 mm and 2.98°C and 664 mm for the low elevation (#604 at 1426m elevation) and high elevation (#657 at 1905m elevation) stations, respectively. Peak stream runoff occurs during the spring as a result of snowmelt and/or high intensity rainfall events. The forest community composition at the research site is dominated by *Pseudotsuga menziesii* (Douglas Fir), *Pinus ponderosa* (Ponderosa Pine) and *Larix occidentalis* (Western Larch) (Rowell et al., 2009). As a consequence of logging operations in the early 1900's, most stands are second-growth and are similar in age (approximately 70 - 100 years old; Hoylman et al., 2018).

2.2. Bedrock attributes

The Proterozoic Garnet Range and Bonner Formations compose the underlying geology of CW watershed (fig. 1a). The Garnet Range Formation is composed of grayish-red, fine to medium grained, meta-sandstone which is interbedded with layers of grayish-red fissile argillite. The Bonner Formation is approximately 500 m thick and is greenish-gray, fine grained, poorly sorted, slightly feldspathic quartzite. Both formations have undergone intense deformation via multiple orographic events (Winston and Link, 1993). The two formations are separated by an east-west trending normal fault that dissects the central axis of the watershed (Ruppel and Lopez, 1984). All CW study hillslopes are underlain by the Garnet Range Formation, henceforth, referred to as “meta-sandstone”.

The Cretaceous Garnet Stock Formation underlays a majority of the NFEC watershed with portions of the periphery consisting of the Garnet Range and Bonner Formations as well as the Cambrian Silver Hill Formation which is composed of Marble. The Garnet Stock Formation consists of phaneritic quartz monzonite that formed during the Late Cretaceous (Brenner, 1968). All NFEC study hillslopes were underlain by the Garnet stock formation, henceforth, referred to as “monzonite”.

2.3. Hillslope characteristics

Three north facing hillslopes were selected in each watershed to characterize the hillslope runoff dynamics. In CW watershed, the largest hillslope A (350,000 m^2) was selected as the site for drilling bedrock wells (fig. 2). The A hillslope was characterized by two convergent hollows with saturated toe slopes that feed a low gradient riparian corridor. The two smaller hillslopes, B (2,900 m^2) and C (23,500 m^2) drain directly to the valley bottom and are not perennially saturated at their bases. The NFEC hillslopes; A (439,000 m^2), B (78,000 m^2) and C (137,100 m^2) are characterized by steep slopes which drain into convergent hollows that experience perennial subsurface soil saturation. We also selected a 60,000 m^2 hillslope, accessible by road, as the site for groundwater well installation (fig. 2).

The hillslopes in CW and NFEC spanned comparable elevation gradients (NFEC: 1243 m - 2043 m; CW: 1161 m - 1900 m) and hillslope grades (NFEC: 6%-34; CW: 8%-30%). Hillslope soils lining both watersheds are classified by the Natural Resource Conservation Service Soil Survey as Typic Haplustalfs (national cooperative soil survey U.S Department of Agriculture, 2001), however soil pit observations revealed CW meta-sandstone derived soils

were slightly finer textured than NFEC monzonite derived soils. Soil depths across both watersheds range from 0.5 -2 m in hollow positions to 0.5 - 1.0m in upslope positions (Hoylman et al. 2018).

3.0. Methods

3.1. Overview of research methods

To measure the hydrologic response of each watershed, we installed a real time distributed network of stream gauges, soil and bedrock wells (fig 3.). We used these data to assess differences in hydrologic response between each watershed and link apparent differences to bedrock driven controls. Then we measured the in-situ bedrock hydraulic conductivity and fracture network geometry in each watershed. We also characterized important hillslope parameters (e.g. surface topography, geology, soil properties and local atmospheric demand) at each soil well location. These parameters were then regressed against metrics of watershed response in a generalized linear model (GLM) to statistically assess differences in watershed response and evaluate the relative importance of bedrock geology and other hillslope parameters.

3.2. Characterizing streamflow

To characterize streamflow in each watershed we installed stilling wells above and below the discharge zone of CW A hillslope and NFEC B hillslope. Stilling wells were constructed by driving a metal post into the stream bed and affixing screened 3.8 cm PVC casing. Wells were labeled NFEC-1, NFEC-2 and CW-1, CW-2, and given a 1 for downstream and 2 for upstream. Stream stage was recorded with a Solinst Level-Loggers (Solinst Mini Water Level Meter, Model 102M, Solinst Canada Ltd. Georgetown, ON, USA) at 1 hr. intervals from 01 April to 30 September 2017. Barometric pressure corrections were applied to all stilling well time series of stage. Manual measurements of stream stage were collected periodically to verify that the water level recorders were accurately recording stage.

Discharge measurements were conducted using a dilution gauging technique (Covino and McGlynn, 2011 and references therein). To conduct a dilution gauging measurement, a known mass of NaCl was injected upstream of the stilling well and a specific conductivity

probe, attached to a data logger (Campbell CR1000 data logger and CS-547A temperature/conductivity probe, Campbell Scientific, Inc., Logan, Utah, United States) measured the NaCl breakthrough curve as it passed by the stilling well. Stream discharge was then calculated by integrating under the breakthrough curve and applying the previously quantified linear relationship between SC and Cl- (1 uS cm^{-1} increase in SC relates to 0.5 g $liter^{-1}$ NaCl) in the following equation:

$$Q = \frac{T_{MA}}{\int_o^t T_c(t)dt} \quad (1)$$

where Q is discharge, T_{MA} is the tracer mass (NaCl) added, T_c is the background corrected tracer concentration and t is time.

Discharge measurements were conducted as many times as possible at each stilling well from 21 March through 28 August 2017 (14 per stilling well in CW and 10 per stilling well in NFEC). Discharge was measured more frequently during snowmelt and recession to capture rapidly changing flow conditions. Each time a discharge measurement was taken the stream stage was recorded. Three replicate trials were performed at each stilling well to determine the relative average measurement error (+- 5.0 %).

For each stilling well, we developed stage discharge relationships (following guidelines by DeGange et al., 1996).

For stilling wells CW-1,2 and NFEC-1 a power law was used:

$$Q = a \cdot h^b \quad (2)$$

For stilling well NFEC-2, a third order polynomial was used:

$$Q = a \cdot h^3 + a \cdot h^2 + a \cdot h \quad (3)$$

Where Q is discharge, a is the coefficient, h is the stage height, and b is the exponent of the power law regression. All rating curves relationships were well correlated (R^2 range: 0.86 - 0.98). All continuous discharge values higher than the maximum measured discharge (0.12 $m^3\ s^{-1}$ NFEC) and (0.02 $m^3\ s^{-1}$ CW) were removed to reduce error in the analysis. An aggradation of the streambed at NFEC-1 stilling well during peak flow (13 June) prompted the development of two rating curves for the NFEC -1 stilling well (01 April - 13 June) and (14 June - 30 September). At each stilling well, time series of discharge were divided by their respective upslope contributing areas to calculate runoff (mm hr^{-1}), these time series were aggregated into a daily mean runoff (mm hr^{-1}) to capture the predominant trend in streamflow across both watersheds.

Using time series of daily mean runoff for each stilling well, we conducted a recession slope analysis derived from the 1-D horizontal Boussinesq equation. This analysis allowed us to assess bedrock driven differences in the subsurface drainage characteristics in each watershed (Brutsaert and Nieber 1977- see for review). The analysis was conducted between 01 July - 31 July as there was no major precipitation events. We used the statistical program Rstudio (R core team 2013, package "stats V 3.5.0") to calculate the recession index (α_{stream}) for each stilling well during the analysis time period using the following equation:

$$-\frac{dQ}{dt} = \alpha_{stream} \cdot Q^{b} \quad (4)$$

Where Q is the discharge from the reservoir as a function of time (t), α_{stream} is a function of the physical dimensions and hydraulic properties of the aquifer and b is a constant (Rupp and Selker 2006). To further quantify the streamflow behavior in each watershed, we used the daily mean runoff time series to calculate the maximum runoff to minimum runoff ratio (MMR_{stream}) for the time period of 01 April to 30 September. Where MMR_{stream} was calculated as:

$$MMR_{stream} = \frac{Maximum\ (mean\ daily\ runoff)}{Minimum\ (mean\ daily\ runoff)} \quad (5)$$

We used the MMR_{stream} values to quantify difference in the magnitude of streamflow response in each watershed and following interpretation by Gardner and others (2010), to infer the dominant subsurface flow paths contributing to streamflow.

3.3. Characterizing watershed geology

We implemented a combination of bedrock drilling, slug tests and outcrop mapping to characterize the bedrock properties of each watershed. We installed five bedrock wells at our research site (4 in CW and 1 in NFEC), labeled CW-GW-1,2,3,4 and NFEC-GW-1 (fig. 2). Adjacent to CW-GW-1,2,3, we installed a soil well to monitor the connection between soil and bedrock flow systems. Well depths ranged from 3.5 m to 10.5 m. CW-GW-1,2,3 were drilled using a bi-cone rotary bit and CW-GW-4, NFEC-GW-1 using a diamond core bit with water as the re-circulating fluid. The soil-bedrock interface was cased with a 10 cm diameter solid PVC conductor and sealed with either bentonite or cement. A smaller 5 cm diameter

hole was then drilled to the completion depth. To finish each well, a 3 cm diameter slotted casing was driven to bottom of the well. Bedrock well elevations were surveyed with a Trimble GNSS Pro XRT (Trimble Inc., California, United States).

For wells drilled below the bedrock water table, water levels were recorded at 1 hour intervals with Solinst Level-loggers. Water levels in CW-GW-1, 2 and 3 were recorded for entirety of research period and NFEC-GW-1 water level was recorded from 16 August - 30 September because installation was not completed until 16 August. The water level was not recorded in CW-GW-4 because of an equipment malfunction. Median water table heights were calculated for each bedrock well where a water level was recorded. Slug tests were conducted in CW-GW-1,2 and NFEC-GW-1 to characterize the rate water flowed through the bedrock in each watershed. They were performed by injecting 3.78 L and recording the falling head with Solinst Level-loggers set at secondly intervals. Bedrock hydraulic conductivity was calculated in m s^{-1} using the Hvorslev (1951) equation:

$$H_t = H_0 \cdot exp(\frac{-K \cdot F}{A \cdot t}) \quad (6)$$

Where A is the cross-sectional area of the well, K is the hydraulic conductivity and F is a shape factor describing the well or piezometer design (here, F= 11 for a cased hole flush with the bottom), and $H_t$and $H_0$are the drawdown ratios at times $t_0$and t_1. We estimated K by fitting the observed drawdown ratio at all times with equation (6) using a Marquart-Levenberg technique (Schwartz and Zhang 2003).

Wells logs were constructed from detailed observations of drill cuttings, fluid circulation and drill speed. As both bedrocks had relatively low matrix porosity yet displayed fracturing, we assessed the geometry of bedrock fracture networks as they were likely the main conduit for water flow. We selected 3 meta-sandstone outcrops in CW and 21 monzonite outcrops in NFEC and mapped the fracture density and connectivity following the methodology of Pahl (1981) and Watkins and others (2015). Only 3 surficial outcrops in the meta-sandstone were present in the CW watershed, thus limiting our mapping efforts.

3.4. Characterizing Shallow Subsurface Flow

Continuous hydrometric measurements of SSF were collected at each study hillslope across both watersheds from 1 April to 30 September 2017. Our observation network consisted of 23 soil wells previously installed at NFEC's A, B and C hillslopes by Hoylman and

others (2018) and an additional 39 soil wells at CW's A, B and C hillslopes (Fig. 2). All soil wells were constructed by inserting a metal rod into a 1.5 m long horizontally screened 3.8 cm diameter PVC casing and driving the metal rod to refusal at the soil - bedrock interface. We applied a bentonite native soil mix to the annulus of each soil well to prevent surface water infiltration. The soil wells were installed systematically along hydrologic flow paths at hollow, side slope and ridgeline hillslope positions to capture the local topographic gradient at each hillslope. All 62 soil wells were instrumented with Tru-Track capacitance rods (Truck-track Inc., Christchurch, New Zealand) or Solinst Level-loggers set at 1 hour intervals.

We used the time series of SSF height for each soil well to conduct a recession slope analysis to assess subsurface drainage characteristics of the soil zone and gain insight into how drainage characteristics may be spatial variable at the hillslope and watershed scales. The analysis was conducted between 14 June - 16 June to capture the drainage of the soil zone after the June 13th 70mm rainfall event. This event was selected because SSF was initiated across all six hillslopes which allowed us to assess the soil drainage characteristics at largest spatial scale possible given our soil well network. However, not all soil wells recorded SSF directly after the June 13th event and the analysis was conducted with 17 soil wells in CW and 13 soil wells in NFEC. We used the statistical program Rstudio (R core team 2013, package "stats V 3.5.0") to calculate the recession index (α_{SSF}) for all 30 soil wells during the analysis time period using (eq. 4). Lastly, using the same statistical package in R studio, we examined inter-watershed differences in the recession behavior with linear regression.

3.5. Parameters governing SSF response

We collected point scale measurements of soil properties, surface topography, local climate and bedrock geology at each soil well. These data were compiled into a set of hillslope parameters which characterized the local conditions at each soil well. However, assessing specific measure of bedrock geology at each soil well presented a logistical challenge so we classified soil wells in each watershed with their respective geologic type (CW: meta-sandstone; NFEC: monzonite) This data set was then used in a statistical analysis (as described below) to assess the significance of each parameter.

To characterize the rate water flowed through the soil zone of each watershed, we measured the in-situ saturated soil hydraulic conductivity (K_{soil}) in each soil well. For perennially saturated soil wells (15 out 62), we conducted a slug test by injecting 1.0 L of water into each well and recording the falling head with Solinst Level-loggers recording at secondly intervals. The time series of falling head were subsequently normalized and the K_{soil} for each well was calculated (in m s^{-1}) using the Hvorslev (1951) method (eq. 6). For wells that were not perennially saturated (47), we used a compact constant head permeameter (CCHP) (KSAT Inc., Raleigh, North Carolina, United States) to determine K_{soil} across a 0.15 m interval at the bottom of each soil well. During operation of the CCHP, a constant head of water was maintained, and steady-state flow rate of water was measured as the CCHP reservoir drained. We calculated (K_{soil} m s^{-1}) for each soil well as:

$$K_{soil} = \frac{Q}{B} \quad (7)$$

Where Q was one measurement of the steady flow rate and B was the surface area of the saturated orb. B was calculated as:

$$B = \frac{3ln(\frac{H}{r})}{\pi H(3H+2s)} \quad (7.1)$$

Where H was the depth of water in the hole, r was the radius of the hole and s was the (estimated) distance from the bottom of the hole to the impermeable layer. (Amoozegar 2001). We then used a Wald Type 2 T-test (R core team 2013, package "AOD V 1.3") to assess if the two watersheds soil properties were significantly different. We also assessed soil depth to understand the degree of soil zone storage in each watershed. Given our soil well installation procedure involved driving a steel rod to refusal, we used the soil well depth as a measure of soil depth at each soil well location.

To characterize the influence of surface topography on the routing of SSF in each watershed we derived a 10m resolution digital elevation model (DEM) from $1m^2$ LiDAR data. A 10m DEM was used in lieu of a finer scale DEM to capture relevant topographic features (e.g. hillslope convergence and divergence) and limit the influence of micro topographic features (e.g. boulders or fallen trees) not likely to influence SSF. Using the 10m DEM and the SAGA GIS program (Conrad et al., 2015), the TWI was calculated as:

$$TWI = ln(\frac{\alpha}{tan(\beta)}) \quad (8)$$

where α is the specific upslope accumulated area for a given point in the watershed and β is the local slope. For the upslope area calculation, we used the multiflow algorithm for flow routing (Seibert and McGlynn, 2007)

We employed a simple climatic water balance (deficit) to represent local climatic conditions at each soil well (Stephenson, 1998). Deficit is the difference between actual evapotranspiration (AET) and potential evapotranspiration (PET) and is calculated in millimeters (Dobrowski et al., 2013). A 250 m deficit product developed by (Holden in prep) was used to calculate a mean annual deficit (mm) value for the previous climatic normal (1981 - 2010) at each soil well location. Although, our soil well network was installed on north aspect hillslopes, the elevation difference between the lowest soil well (CW-C -2 at 1318 m) to the highest soil well (NFEC - A -7 at 1730 m) suggested the use of a gridded data to capture spatial differences in the local climatic conditions.

3.6. Statistical analysis

We used generalized linear modelling (GLM) to determine if the shallow subsurface flow (SSF) response of each watershed was statistically different. We also used this analysis as a hypothesis testing tool to investigate the link between SSF response and the bedrock geology of each watershed. Furthermore, because GLM's can be multivariate, this analysis allowed us to develop a hierarchical understanding of which soil well parameters (as described in section 3.5.) exerted the strongest control SSF response across each watershed.

To conduct this analysis, we utilized the GLM function found in the statistical program RStudio (R core team 2013, package "stats V 3.5.0"). We used a GLM in lieu of multiple linear regression (MLR) to accommodate our response (dependent) variables which did not fit a normal distribution (mean ≠ 0) and were not continuous (e.g. proportions). Unlike an MLR which assumes a normal distribution, a GLM incorporates the exponential family of distributions (Dobson and Barnett 2008 see for review of exponential distribution family). This feature of the GLM framework was useful in this analysis as the distribution of our response variables fit within the exponential family classification. The basic set of GLM equations were pulled from Dobson and Barnett 2008 and are as follows:

$$E(Y_i) = u_i \tag{9}$$

$$g(u_i) = (\chi_i^T \cdot \beta) \tag{9.1}$$

In (eq. 9), $E(Y_i)$ is the expected outcome of the response variable and is assigned the appropriate distribution from the exponential family and u_i is a function of each predictor variables χ_i^T and unknown parameters β. In equation 9.1, g is the link function which allows u_i to be linearly related to χ_i^T and β.

For all 62 soil wells, we quantified two response variables using each recorded time series of SSF. The first SSF response variable was the duration of time SSF recorded at each soil well and was calculated as a proportion:

$$\hat{P}(SSF) = \left(\frac{Observations_{SSF}}{Observations_{Total}}\right) \quad (10)$$

Where the proportion of shallow subsurface flow $\hat{P}(SSF)$ was equal to the number of observations when water was present in a soil well ($Observations_{SSF}$) divided by the total number of observations recorded at each soil well over the study period ($Observations_{Total}$). Given a proportion is bounded between 0 and 1, we assigned this response variable (eq. 10) a distribution from binomial family (sub-family to exponential family) and the appropriate link function (eq. 9.1).

The second response variable was average height of SSF recorded at each soil well and was calculated as:

$$Scaled\ Median\ SSF\ Height = \left(\frac{Median\ SSF\ Height\ (m)}{Soil\ Well\ Depth\ (m)}\right) \quad (11)$$

The median height SSF was calculated instead of the mean to account for skewness in soil well data sets and was then scaled by the soil well depth (1 = water at soil surface, 0 = dry well) to account for varying depths of each soil well. We assigned this response variable (eq. 11) a distribution from the gamma family (sub-family to exponential family) because the distribution was continuous and bounded above zero and assigned the appropriate link function (eq. 9).

To understand what parameters governed the proportion (eq. 10) and height (eq.11) of SSF, we characterized a set of 5 parameters at each soil well (as described in section 3.5) and used them as predictor variables (χ_i^T). The set of five predictor variables were then regressed against each response variables (Y_i) in two separate analyses using an automated stepwise function (R core team 2013, package “stats V 3.5.0”). The automated stepwise function evaluates all possible model permutations and seeks to minimize the residual deviance (measures goodness of fit in a model) and Akaike Information Criterion

(AIC) value. The combination of fewest predictors with smallest amount of residual deviance was then selected by the stepwise function as the most parsimonious model for each separate analysis. As a final model selection process, we used a Wald Type 2 T-test (R core team 2013, package "AOD V 1.3") to assess the significance each predictor variable selected for both final models and removed any predictor that was not significant ($p > .05$).

4.0. Results

4.1. Analysis of streamflow hydrographs

Qualitatively, the North Fork Elk Creek (NFEC) stream was more responsive and dynamic compared to the Cap Wallace (CW) stream (fig 4.). The NFEC stream responded rapidly to events and exhibited high runoff during the spring and low runoff during the summer with the maximum to minimum flow ratio (MMR_{stream}) ranging from 62.50 to 137.48 (fig. 4c,d). Conversely, the CW stream maintained relatively uniform flow conditions with minor fluctuation throughout the season with the (MMR_{stream}) ranging from 5.33 to 8.58 (fig. 4a,b). The hydrograph recession slope analysis revealed faster rates of subsurface drainage in the NFEC stream relative to the CW stream. The average stilling well recession index (α_{stream}) for the NFEC stream was an order of magnitude greater compared the average stilling well (α_{stream}) for the CW stream (NFEC: -3.00 x 10^1; CW: -7.00 x 10^2) (fig. 4b,d).

4.2. Analysis of bedrock parameters

Qualitatively, the monzonite bedrock underlying the NFEC watershed had lower numbers and less connected fractures compared to the meta-sandstone underlying the CW watershed (fig 5a,b). The mapped fracture density of the monzonite bedrock underlying NFEC (7.4 fractures m^{-2}) was approximately 6.3 times lower than the meta-sandstone bedrock underlying CW (46.5 fractures m^{-2}) (fig 5.). Like the difference in fracture density, the number of connected fractures in the monzonite bedrock (4.1 connected fractures m^{-2}) was also approximately 8 times lower than the meta-sandstone bedrock (31.3 connected fractures m^{-2}) (fig 5.). The hydraulic conductivity in the NFEC bedrock well (4.4 x 10^{-5} m s^{-1}) was an order of magnitude higher than the averaged hydraulic conductivity from the two CW bedrock wells (2.2 x 10^{-6} m s^{-1}) (fig. 5).

Detailed well logs and drill operator observations revealed that meta-sandstone bedrock of CW was easier to penetrate with the drill then the monzonite bedrock of NFEC (fig. 5). We recorded drill rates between 0.1 m min $^{-1}$ to 0.3 m min $^{-1}$ in the meta-sandstone and drill rates of 0.01 m min $^{-1}$ to 0.1 m min $^{-1}$ in the monzonite. Drill rates in the meta-sandstone were extremely variable and it was typical for drill rate to be slow and then rapidly increase. After the drill rate increased, the circulation rate of the drilling fluid immediately decreased. Furthermore, core recovery was minimal during CW GW - 4 drilling and only 0.05 m was successfully extracted. Drill rates in the monzonite were relatively consistent throughout and a typical core filled the length of the core barrel (1 m). Qualitative observations of the monzonite core revealed minor oxidation staining and sub-vertical micro fractures. Fluid circulation was relatively constant until we reached 6.5 m depth, after which, it was difficult to maintain circulation for the remainder drilling operations at the NFEC GW -1 well site.

4.3. Analysis of paired soil and groundwater wells

In the CW watershed, we observed varying degrees of hydrologic connection between soil and bedrock flow systems (fig. 6). In (fig. 6a), the two flow systems mimicked each other throughout the spring and the vertical flux of water was limited. In (fig. 6b), the response of the soil flow system was entirely dependent of the rate and timing of bedrock groundwater exfiltration into the soil zone. Rain and melt events spawned flux between the two systems even for short periods of time (fig. a,b). In (fig. 6c), only the bedrock flow system responded to rain and melt events while the overlying soil zone remained unsaturated. The bedrock water levels were not static, with rises recorded of greater than 3m (fig. 6c). The two paired sets of soil and groundwater wells (fig. 6a, b) were in a hollow while the pair that did not show a connection was located on a nose (fig. 6c - see fig.2 for exact locations). Showing that bedrock flow systems were more connected with soil flow systems in areas of convergence such as the base of a slope rather than in areas of divergence such as the nose of slope.

4.4. Analysis of soil well recession and response magnitude

The side slope SSF response across both watersheds displayed transient behavior, in contrast, the hollow SSF response across both watershed displayed perennial behavior(fig

7.). However, the NFEC hollow soil wells rose rapidly in response to rain and melt events and continually drained late into the summer (fig. 8b), while ,the CW hollow soil wells exhibited a muted response and maintained relatively constant levels late into the summer (fig. 8a). The maximum to minimum flow ratios (MMR_{SSF}) for each soil well show this difference in response dynamics as the average $MMR_{SSF}$for all soil wells included in this analysis was 108.20 for NFEC and 38.70 for CW (table 1a,b). In (fig. 8c,d), the recession index (α_{SSF}) values for the NFEC hollow soil wells were higher compared to CW hollow soil wells, while, the α_{SSF} values for side slope positions were comparable. The regression lines in (fig. 8c,d) capture this divergence in hollow soil well α_{SSF} values and indicate that subsurface drainage rates between side slopes and hollows varied less in the NFEC relative to CW.

4.5. Analysis of watershed shallow subsurface flow response

In simple terms, the soil zone in the monzonite watershed (NFEC) was statistically "wetter" relative to the soil zone in the meta-sandstone watershed (CW). The bivariate plots in (fig. 9a, b), highlight this result and show the relationship between a) proportion of time and b) average height of shallow subsurface flow (SSF) and topographic wetness index (TWI). Specifying, that for a given TWI value, SSF was more likely to occur for longer time periods and at greater heights in the soil zone of the NFEC watershed compared to the CW watershed (fig. 9a,b). When hillslopes in both watersheds accumulated drainage area and transitioned from steep upslope areas to hollow areas the duration and height of SSF increased exponentially (fig 9a,b). The colored regression lines in (fig. 9a,b) show the strong relationship between surface topography and a) proportion of time and b) average height of SSF across both relationships (a) P<.05 b) P<.05. This effect of surface topography on the spatio-temporal distribution of SSF is summarized in (fig. 7), where each soil well was assigned its corresponding TWI value which was then used to plot a binary time series of the observed the proportion of time a soil well recorded SSF.

While the bivariate plots in (fig. 9a, b) illustrate the relationship between SSF and surface topography, results from the generalized linear modeling (GLM) analysis showed the proportion of time a soil well would record SSF increased in areas with greater TWI values and underlain by monzonite bedrock (Coefficients: +1.59 TWI; + 4.11 geology: NFEC). These two parameters explained 84% of the total deviance and showed that surface topography

and bedrock geology played a considerable role in controlling the proportion of time SSF occurred across these watersheds (table 2a).

The model best fitted to predict the scaled median height of SSF included TWI, geology: NFEC and deficit. The scaled median height of SSF became greater as TWI increased, when soil wells were underlain by monzonite and the deficit (proxy for atmospheric demand) was reduced (Coefficients: +.44 TWI; +.85 geology: NFEC; -.02 Deficit). The inclusion of the deficit parameter in this model indicated that the height of SSF was more sensitive to changes in atmospheric demand compared to proportion of SSF. These parameters explained 62 % of the total model deviance and showed that surface topography, watershed geology and deficit in part all governed the average height of SSF across both watersheds (table 2b).

5.0. Discussion

5.1. Assessing bedrock controls on streamflow response

The field of watershed hydrology has made great progress in disentangling the high degree of complexity associated with watershed runoff response (Pfister et al.,2017) and researchers have identified bedrock permeability as a key control of streamflow response in headwater catchments (Uchida et al., 2006). In this study, we observed a striking difference in the magnitude of stream runoff for each watershed (fig. 4a, c). The NFEC stream underlain by monzonite bedrock, showed large variations in runoff (fig. 4c) while the CW stream underlain by meta-sandstone bedrock, displayed minor fluctuation in stream runoff (fig. 4a). Runoff ratio calculations revealed the average MMR_{strean} was 10 times lower in the CW stream relative to the NFEC stream (fig 4b,d). Given these two watersheds share a ridge line, similar weather patterns and topographic form, the difference in streamflow response was surprising. To investigate this discrepancy, we conducted a streamflow recession slope analysis for each watershed to link the streamflow response to subsurface drainage characteristics.

The streamflow recession slope analysis revealed that the subsurface drainage in the CW watershed was much slower than in the NFEC watershed. For example, the average CW α_{stream} was an order of magnitude lower than the average NFEC α_{stream} (fig. 4b,d). This

analysis suggests that the subsurface properties of each watershed influenced the rate and volume of hillslope discharge to the adjacent stream. However, we acknowledge that only relying on records of streamflow as a basis for subsurface interpretation can be misleading (Hale and McDonnell 2016a). For example, Hale and McDonnell (2016a) observed strikingly similar hydrographs responses between two catchments underlain by dissimilar geologies, however, they recorded a 4 years' difference in the mean transit time of stream runoff. To account for this, we quantified the bedrock properties of each watershed to assess this divergence in streamflow and strengthen our interpretation.

Analysis of bedrock properties revealed considerable differences in the monzonite and meta-sandstone fracture geometries and hydraulic conductivities (fig 5.). The increased runoff response in the NFEC stream was likely a function of the widely spaced and highly conductive fracture network in the monzonite bedrock (Uchida et al., 2002). When hydrologically active, the monzonite fracture network promoted rapid drainage of groundwater and acted similarly to macro pores (McDonnell 1990) or more generally preferential flow paths in the soil zone (Anderson et al., 2009). Conversely, the meta-sandstone had a highly connected fracture network with lower conductivity relative to the monzonite. The meta-sandstone fracture network act like a matrix driven flow system (i.e. greater effective porosity relative to the monzonite) which promoted a subdued stream runoff response. These results align with observations of Uchida and others (2006), who found baseflow recession curves became subdued with increased dynamic bedrock storage. Furthermore, we echo suggestions from Tague and Grant (2004) and suggest that the unique properties of the underlying bedrock governed the streamflow response in both watersheds.

5.2. Assessing the bedrock controls on hillslope runoff generation

To understand the role of bedrock in upland runoff generation, it was critical to investigate the connection between soil and bedrock flow systems. For years, hillslope hydrologists have debated to what degree soil and bedrock flow systems interact and have acknowledged that the boundary between the soil and bedrock is of utmost importance in shallow subsurface flow (SSF) generation (Tromp Van Meerveld 2006a, b; Hopp and McDonnell, 2009; Graham et al., 2010). However, given the logistical challenge of installing

groundwater wells in mountain watersheds few observations documenting connections between soil and bedrock flow systems have been made (Gabrielli et al., 2012).

We installed 5 bedrock groundwater wells across both watersheds out of which 3 had adjacent soil wells. Observations from these paired soil-bedrock wells were instrumental in broadening our understanding of the connection between soil and bedrock flow systems. In 2 pairs of soil-bedrock wells located in convergent hollow areas, we recorded an upward and downward vertical flux of water between bedrock and soil flow systems (fig. 2; fig. 6a, b), indicating water from each reservoir was likely mixing at the slope base. These were not the first observations of bedrock exfiltration occurring at the slope base, for example Uchida and others (2003) measured the flux between bedrock and soil in downslope positions at their Fudoji research site in Japan. At the soil-bedrock well nest located on a divergent nose area, we did not observe a connection between soil and bedrock flow systems, instead, recorded large fluctuations (> 3m) in the bedrock water table while the soil zone remained unsaturated (fig. 6c). These dynamic responses in the bedrock water table were likely a function of upslope flow paths recharging the bedrock reservoir which when combined with the soil zone acted as an unconfined aquifer system.

Our observations provide strong evidence that areas of topographic divergence are likely groundwater recharge zones while areas of topographic convergence are groundwater discharge zones (Wilson and Dietrich 1987). For example, the vertical flux of water between soil and bedrock zones was only documented in hollow locations (fig. 6a,b) however, in one well pair there was a leaky confining layer that separated the two zones of saturation (fig. 6b). Others prior have observed groundwater exfiltration to overlying soil through fractures (Anderson et al., 1997; Uchida et al., 2003). For example, Kosugi and others (2006) recorded exfiltration from the bedrock toward the soil layer composed more than half the annual hillslope runoff in an unchanneled headwater catchment. While groundwater exfiltration is likely a dominant source of hillslope runoff, it is likely a more common hillslope runoff mechanisms in convergent hollows (fig. 6a,b). Our results suggest that the bedrock characteristics and topography of a watershed which govern the rate and volume of groundwater exfiltration may heavily influence spatial patterns of hillslope runoff generation.

To test the influence of groundwater exfiltration on SSF response across both watersheds, we conducted an SSF recession slope analysis after a large rain event to

determine if the influence of monzonite and meta-sandstone bedrock would be evident in soil drainage response of each watershed. Given our analysis of soil properties revealed there was not a significant difference in the soils hydraulic conductivity ($p > .05$), we hypothesized that bedrock controls would promote differences in hillslope drainage characteristics between each watershed. From this analysis, it was evident the hollows in NFEC drained faster relative to the hollows in CW, however, we did not observe a difference in drainage characteristics across upslope regions. (fig.8 c, d). Furthermore, the NFEC soil zone had a substantially higher average MMR_{SSF} indicating the height of SSF drainage was more dynamic (table 2a,b).

We suggest the upslope soil wells displayed similar drainage characteristics because they had less interaction with deeper bedrock flow systems (i.e. perched shallow subsurface flow). Thus, the upslope soil drainage characteristics were likely more controlled by mechanisms such as macro pore flow (McDonnell, 1990; Sidle et al., 2001), not bedrock properties. However, as hillslopes transitioned from upslope to downslope regions, we observed a divergence in hollow α_{SSF} values between each watershed (NFEC > CW). It appears the conductive fracture network in the monzonite bedrock facilitated rapid hillslope discharge, while the less conductive fracture network in meta-sandstone bedrock limited rates of hillslope discharge (fig 5; fig 8 a,b), hence, promoting long term storage in the groundwater system. Both recession analyses revealed that the bedrock properties of a watershed influence not only the streamflow response but also hillslope runoff generation processes.

5.3. Assessing the influence of hillslope parameters on shallow subsurface flow (SSF) response

When saturated zones formed and SSF was initiated across our study watersheds (Weyman 1973; Whipkey 1965; Bachmair and Weiler,2011; see for review of SSF initiation), it was likely a portion of SSF percolated into the underlying bedrock. Given recent estimations of 14-44% (Aishlin and McNamara 2011) and 21% (Graham et al. 2010) of annual precipitation percolates into bedrock flow systems, we hypothesized that inter-watershed variability in deep percolation rates at the soil bedrock interface would cause a difference in the height and proportion of SSF response. In each comparative analysis, the

SSF response across soils wells underlain by monzonite bedrock (NFEC watershed) was statistically greater ($P < 0.05$) (table 2 a,b). These analyses indicated that to some degree the soils in the NFEC watershed were more hydrologically active than the soils in the CW watershed(fig. 9 a,b) likely a result of less percolation in the NFEC watershed. While our deep percolation hypothesis may be plausible, the selection of other hillslope parameters such as surface topography and deficit suggest other parameters besides bedrock geology also played a role in controlling the SSF response of each watershed.

As the flow of water, which at the watershed scale generally follows topography (Sorensen and Siebert, 2007), it is not surprising we documented a strong link between topography and watershed scale patterns of SSF response, as have many others (Burt and Butcher, 1985; Anderson and Burt, 1978; Jencso et al., 2009; Rinderer et al., 2014). The statistical analysis revealed topographic gradients (described with TWI) were a significant factor driving the proportion and height of SSF in each watershed (TWI: $P< .05$). This finding corroborates with Rinderer and others (2014), who predicted soil water levels across 51 monitoring sites using the topographic metric TWI ($r^2 > 0.6$) and found water table heights in zones with large upslope contributing areas and low slopes tended to be higher and more persistent. Others (Haught and Van Meerveld, 2011; Seibert et al., 2003), have recognized the existence of distinct hydrologic regions (upslope vs. downslope), where transient patterns of SSF in upslope regions subsidize perennial patterns of SSF in downslope regions. Furthermore, deeper flow paths that emerge at the slope base provide an additional source of SSF in downslope regions. As shown in this study, TWI can accurately capture spatially organized patterns of SSF as promoted by both shallow and deep subsurface flow paths in watersheds of differing bedrock geology.

Areas of topographic convergence will typically have increased moisture conditions due to unsaturated gravitational drainage of upslope soils zones (Western et al., 1999). While we did not measure soil moisture conditions directly, we did use a climatic water balance to quantify the atmospheric demand on soil water storage at each soil well. As a result, soil wells located in higher deficit regions had decreased heights of SSF compared to soil wells located at lower deficit regions (table 2b.). This was likely due to the topo-climatic patterns resulting from elevational differences across the study areas. For example, soil wells at higher elevations may have experienced increased precipitation due to an orographic effect. These observations support findings from Hoylman and other in prep,

who conducted a finer scale investigation of topo-climatic gradients in the NFEC watershed and found spatial patterns of subsurface flow durations were highly related to the atmospheric demand on soil water storage.

6.0 Implications

As runoff in headwater catchments is effectively the result of the upland soil and bedrock reservoir drainage, it is likely that the subtle differences in inter-watershed SSF response may be interconnected to the differences we observed in soil well (α_{SSF}) and MMR_{SSF} values. For example, slower exfiltration of groundwater in the CW hollows may have promoted a more stable SSF response (fig. 8a), conversely, more rapid exfiltration of groundwater in the NFEC hollows may have led to a more dynamic SSF response (fig. 8b). Ultimately, to some degree a stream is an aggregation of multiple hillslopes and through our measures of bedrock properties and streamflow analysis it evident that as hillslopes become nested within a watershed, the relative role of bedrock geology increases.

To conceptualize these results, let us consider the 2-D vs. 3-D streamflow generation conceptual models developed by Frisbee and others (2012 - see for review). The NFEC watershed supports the 2-D conceptualization, were streamflow generation is likely an aggregation of shallow lateral subsurface flow paths in highly conductive bedrock. A 2-D watershed may be highly susceptible to short term changes in seasonal precipitation inputs and likely rely on limited stores of groundwater to supply baseflow. On the other hand, the CW watershed likely favors a 3-D conceptualization, where large networks of interconnected fractures create vertical subsurface flow paths and a more developed groundwater system that is controlled by large-scale groundwater flow paths as well as shallow subsurface flow paths. This study reiterates thoughts by Tague and Grant (2004), for which a better understanding of streamflow generation may be accomplished through classifying landscapes by the physical and hydraulic properties of their underlying bedrock.

7.0. Conclusion

This study was spurred by a simple idea, if we monitor the SSF and streamflow response of two adjacent watersheds underlain composed of different geologies, will the runoff response be similar or unalike or a combination of the two? Findings from this study indicate that topographic gradients, represented by TWI, were strong predictors of the

height and duration of SSF across our research site (fig. 9 a,b). As SSF accumulated in the locations of low potential, the storage and release of hillslope water to the adjacent stream became more strongly controlled by the underlying bedrock properties. While both watershed soils shared similar properties, their bedrock properties promoted different runoff responses. We suggest that given our findings and those of others, watersheds underlain by highly permeable bedrock will likely have increased catchment mean transit time (Hale and McDonnell, 2016 b), greater catchment storage (Pfister et al., 2017), reduction in the stream water balance and gross gains (Bergstrom et al., 2016) and more active groundwater circulation controlling the streamflow response (Gardner et al., 2010). Furthermore, we suggest that it is crucial watershed hydrologists adopt a conceptual model of watershed function where dynamic changes in bedrock storage are a well characterized (Hale and McDonnell 2016 b) or else governing mechanisms in streamflow generation may be overlooked.

Future work at this paired watershed research site, will focus on examining the hydrologic connection between bedrock and soil reservoirs. Given our extensive soil well network, we propose installing nested groundwater wells adjacent to each soil well like the study design of Gabrielli and others (2012). By nesting groundwater wells adjacent to soil wells, we will monitor the connection between bedrock and soil flow systems, potentially identifying the spatial organization of this difficult to monitor SSF generation mechanisms. Furthermore, this study bolsters the growing number of watershed comparison studies (Hale and McDonnell 2016 a,b; Gabrielli et al., 2012; Pfister et al., 2017; Uchida et al., 2006), focused on creating a deeper understanding of bedrock geologies role in watershed-scale function.

8.0 Figures

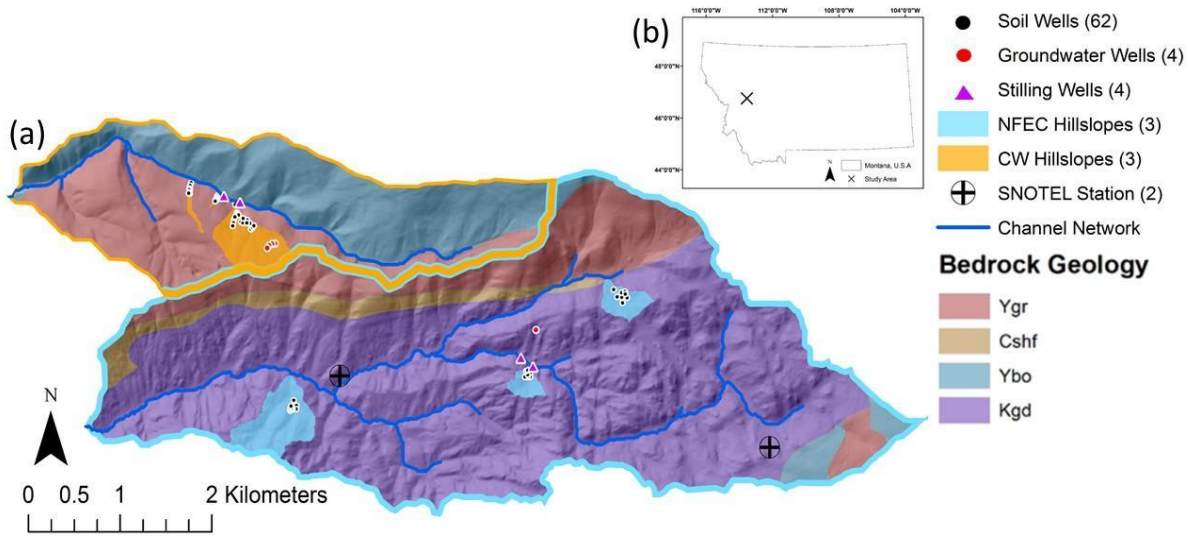

Figure 1. (a) Geologic map of nested study watersheds with hillslope locations and instrumentation. **(b)** Location of study watersheds in the Rocky Mountains, Montana. Bedrock geologic formations that underlay the study watersheds are Garnet Range Formation (Ygr), Silver Hill Formation (Cshf), Bonner Formation (Ybo) and the Garnet Stock Formation (Kgd).

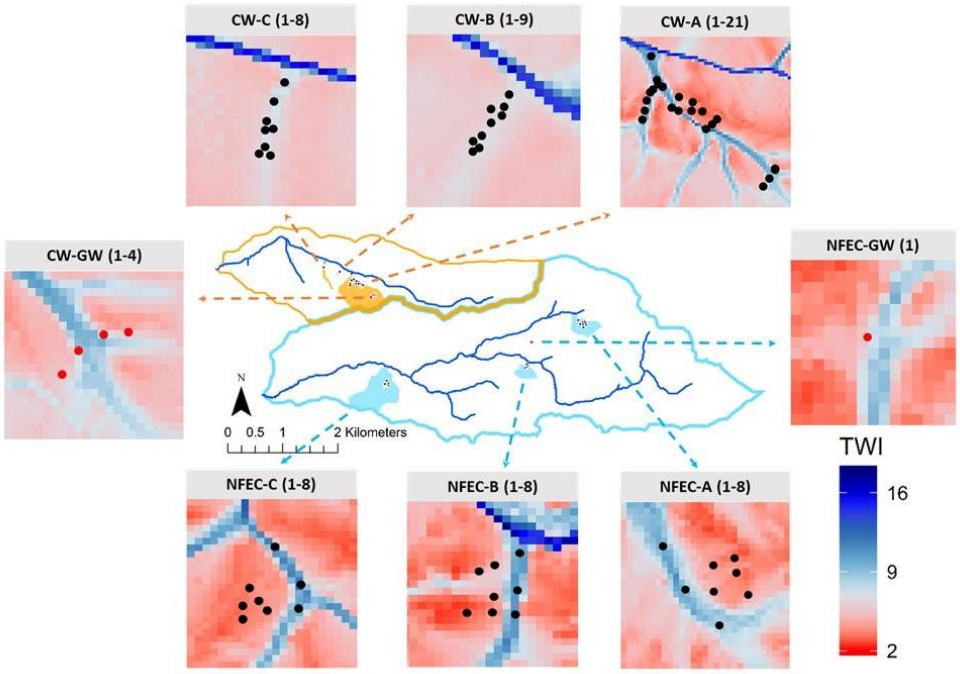

Figure 2. Twi inset maps of CW (A, B, C) and NFEC (A, B, C) with soil and groundwater well locations. NFEC groundwater well (1) was installed on the south facing hillslope across from NFEC B hillslope. CW groundwater wells (1-4) were installed across CW A hillslope. The orange and blue solid lines outline the CW and NFEC watersheds. The black scale bar is assigned to the watershed map.

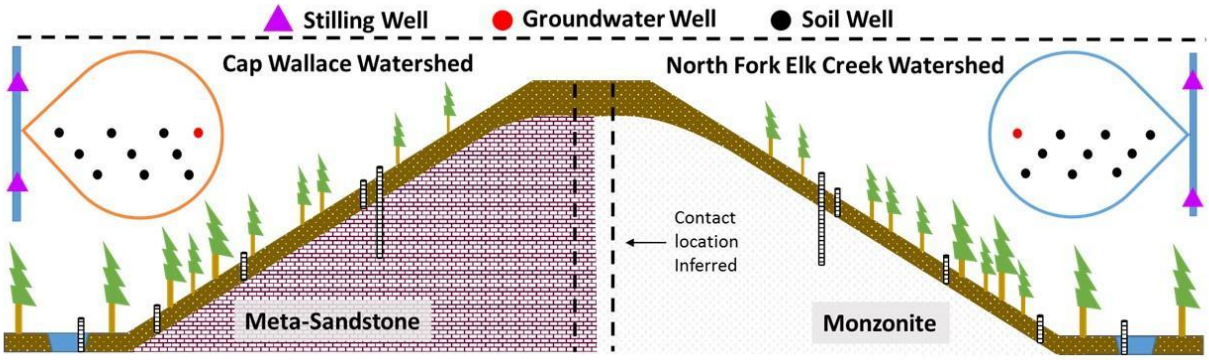

Figure 3. The central animation represents the experimental design in cross section view and the upper left and right animations depict the experimental design in plain view. **(a)** Soil, **(b)** regolith, **(c)** Garnet Range Formation and **(d)** Garnet Stock Formation. White cylinders represent hydrometric measurement locations that span a range of topographic (hollow, side slope and ridge) and hydrologic environments (stream, soil and bedrock).

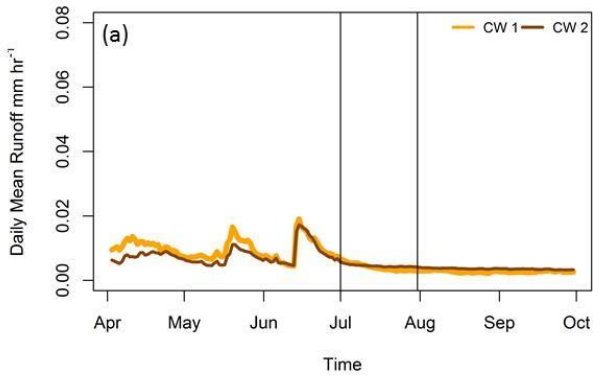

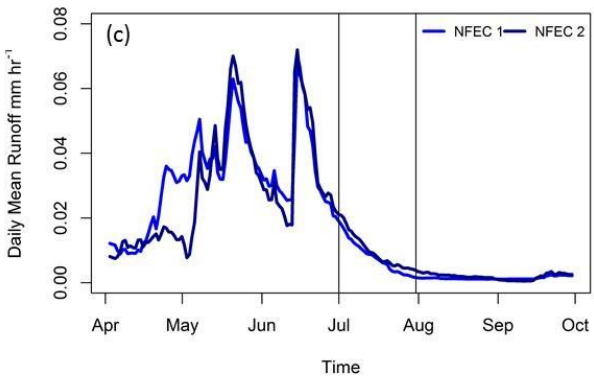

(b) NFEC	MMR	α_{stream}
Stilling Well		
NFEC - 1	62.50	-3.53×10^{-1}
NFEC - 2	137.48	-2.53×10^{-1}
Average	99.99	-3.00×10^{-1}

(d) CW	MMR	α_{stream}
Stilling Well		
CW - 1	8.58	-1.12×10^{-1}
CW - 2	5.33	-2.86×10^{-2}
Average	7.00	-7.00×10^{2}

Figure 4. Plots showing the stream response for both watersheds. The colored lines in **(a)** CW and **(c)** NFEC are time series of stream runoff, where the y – axis is runoff mm hr^{-1} and the x- axis shows the study period in months. The vertical black lines represent the recession analysis time period. Tables **(b)** CW and **(d)** NFEC report the MMR and recession index (α_{stream}) calculated for each stilling well as well as the respective averages for each watershed.

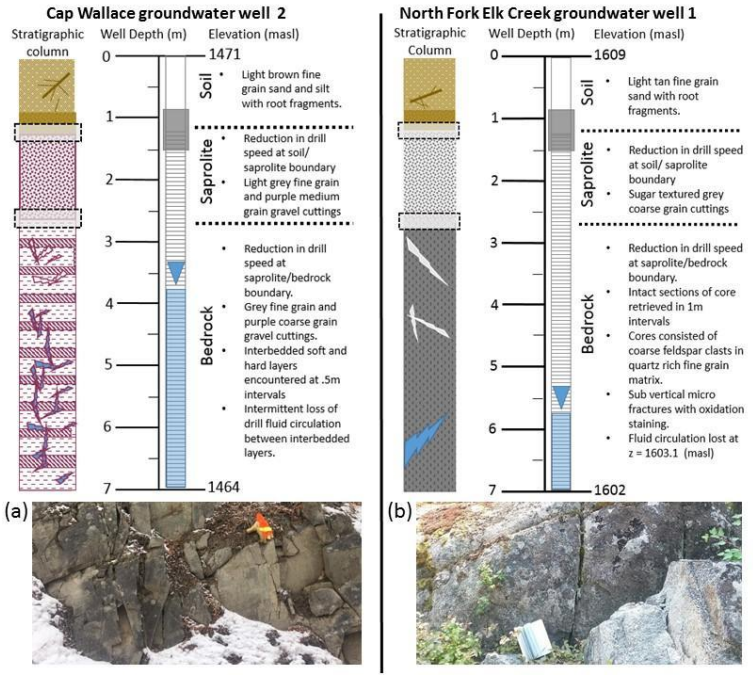

Bedrock Property	Cap Wallace	North Fork Elk Creek
Hydraulic conductivity ($m\ s^{-1}$)	*2.1 x 10^{-6}**	4.4 x 10^{-5}
Fracture density (# m^{-2})	46.5	7.4
Connected fracture density (# m^{-2})	31.3	4.1

* Represents the average hydraulic conductivity between two groundwater wells

Figure 5. The reconstructed stratigraphic columns were developed from field observations and sampling during the drilling process. The black dashed rectangles represent inferred boundaries between soil, saprolite and bedrock. The screened cylinders show final well construction design and the blue triangles show the median water table measured during the study period for the respective wells. Photo **(a)** is an outcrop of the Garnet Range Formation. Photo **(b)** is an outcrop of the Garnet Stock Formation.

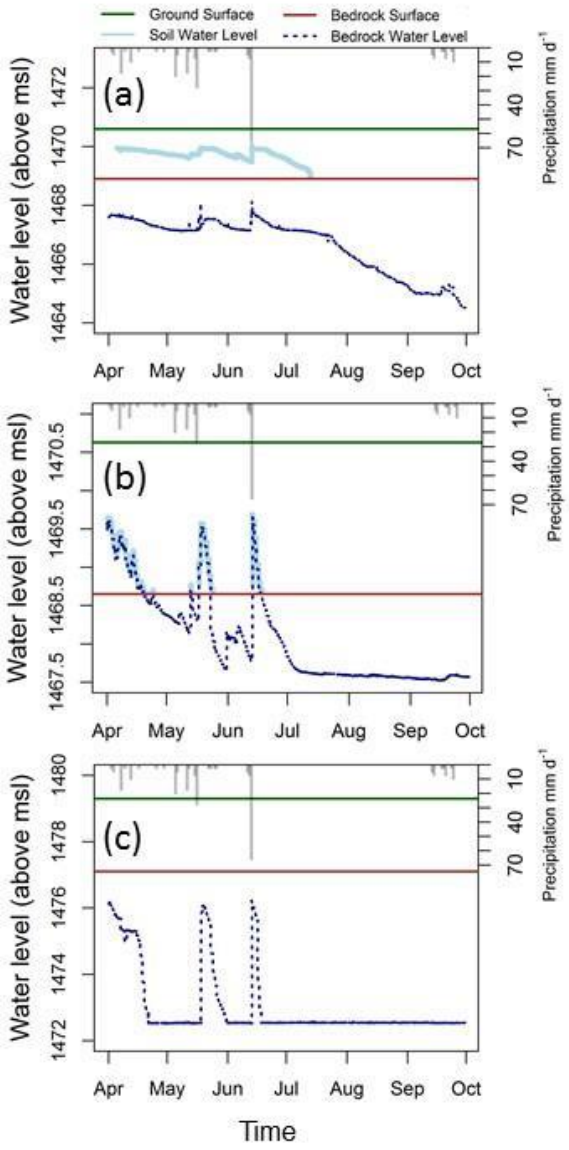

Figure 6. Plots showing the connection between nested bedrock groundwater and soil water well responses recorded in the CW watershed. The X axis shows the study period in months, the primary Y axis is recorded water level (meters above sea level) and the secondary Y axis is daily accumulated precipitation in millimeters. Plot **(a)** CW-GW-1 paired with CW-A- 19, the bedrock and soil well water tables were separated by a leaky confining layer. Plot **(b)** CW-GW-2 paired with CW-A-20, the bedrock and soil well acted as one unconfined flow systems. Plot **(c)** CW-GW-3 paired with CW- A -21, the bedrock well fluctuated up to 3 meters while the soil well did not saturate.

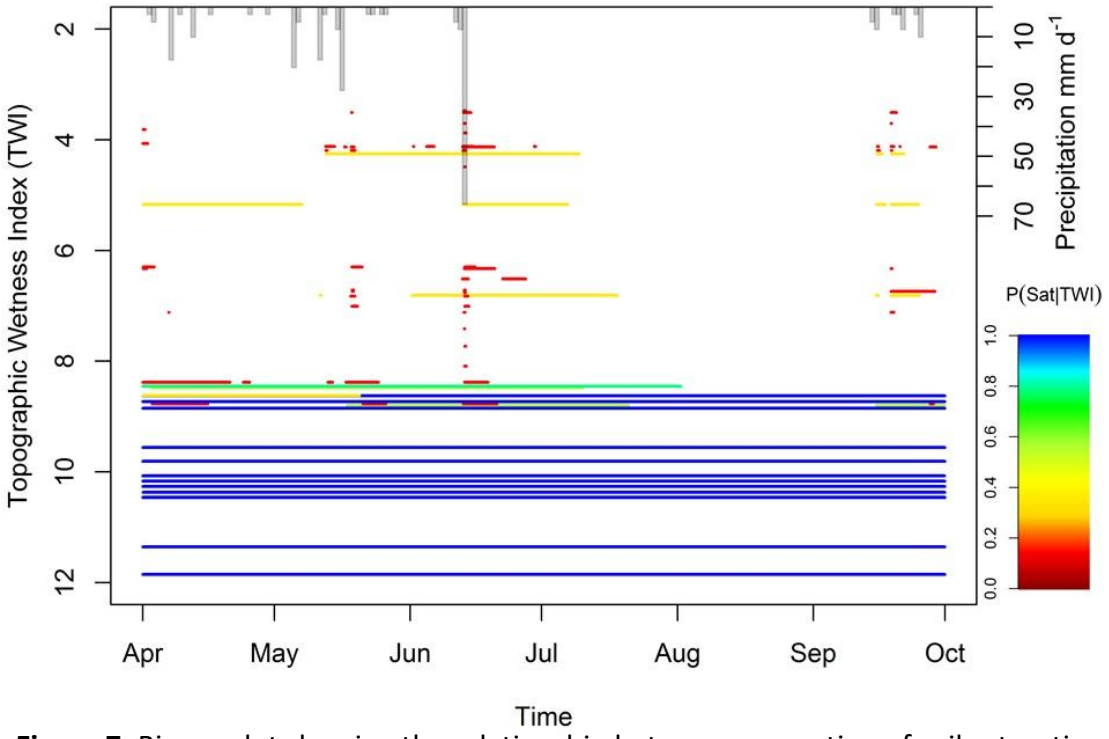

Figure 7. Binary plot showing the relationship between proportion of soil saturation and TWI through the duration of the study. The colored lines represent the proportion of saturation for all soil wells with respect to the assigned TWI for each soil well. The primary Y axis is TWI and the secondary Y is daily accumulated precipitation in millimeters. The X axis shows the study period in months. The proportion of soil saturation is highest in locations with a TWI value greater than 8.

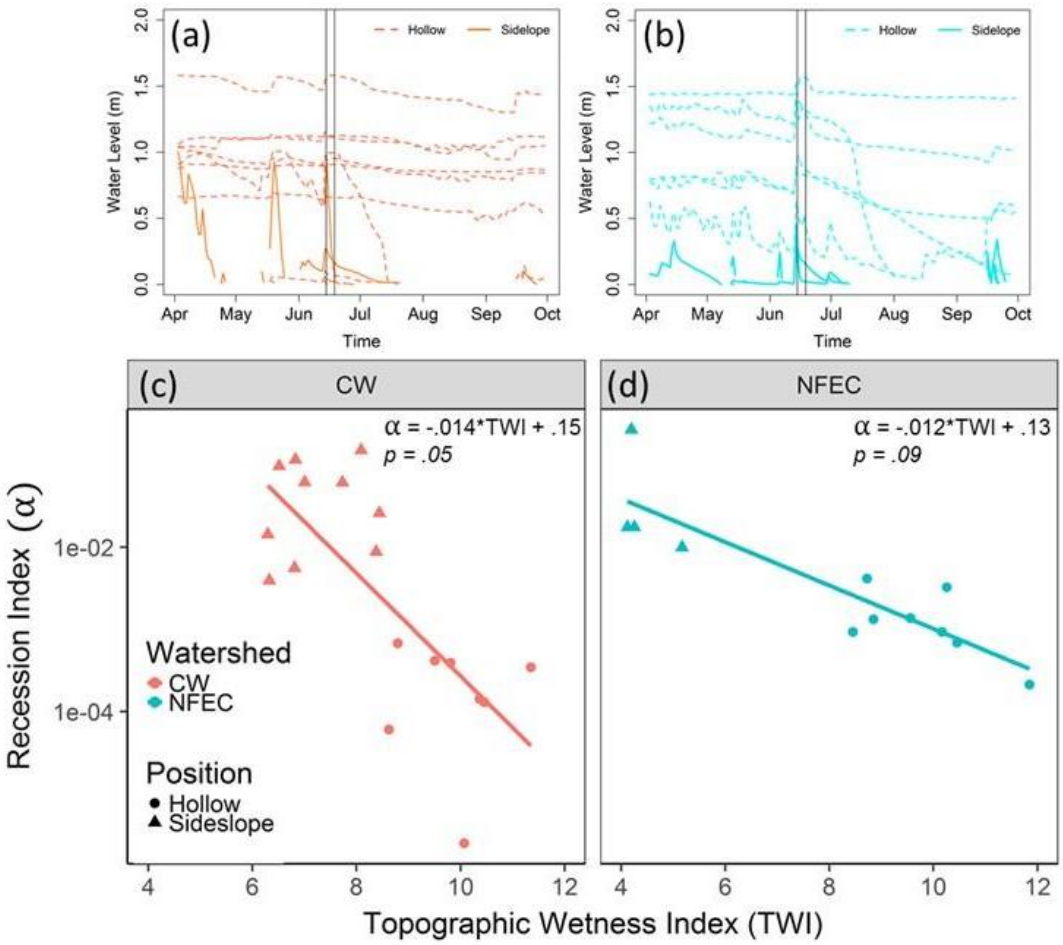

Figure 8. In plots, **(a)** CW and **(b)** NFEC the colored lines are time series of SSF response. Dotted lines are hollow water levels and solid lines are side slope water levels. These time series correspond with the data points shown in plots **(c)** and **(d)**, where triangles are side slope soil wells and squares are hollow soil wells. In plots **(c)** and **(d)**, Y axis is recession index and TWI. Recession index values were calculated during a soil drainage period (denoted by the vertical black lines in plots **(a)** and **(b)**.

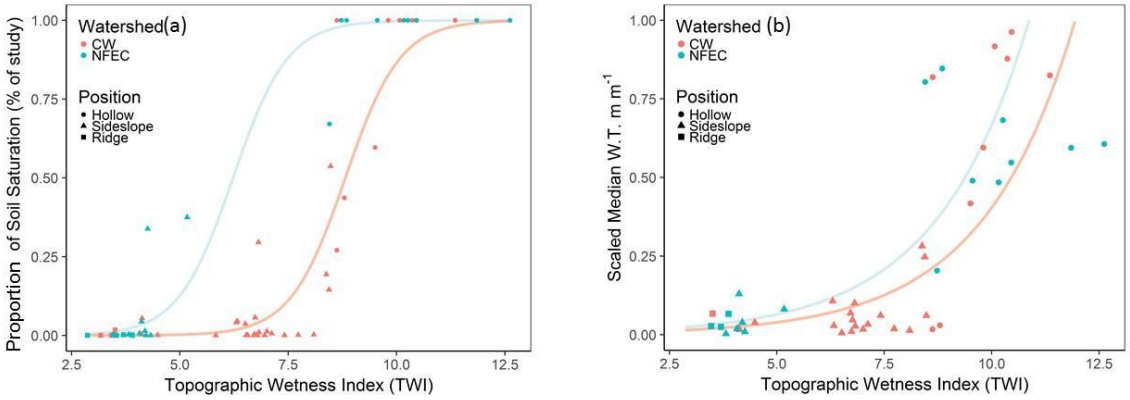

Figure 9. Plots showing the relationship between TWI and SSF metrics **(a)** probability of SSF and **(b)** scaled median water table height. The blue and orange regression lines show each SSF metric as a function of TWI for both watersheds, respectively. The position symbols represent the hillslope position of each soil well.

Table 1. Summary table for MMR and recession values for CW and NFEC **(a)** hollow soil wells and **(b)** stilling wells. Recession slopes were generally lower in hollow locations in the CW watershed.

(a) Cap Wallace	MMR	Recession Index (α)
Soil Well		
A - 1	1.31	-1.42×10^{-4}
A - 2	1.2	-3.45×10^{-4}
A - 3	1.27	-3.92×10^{-4}
A - 4	1.44	-3.20×10^{-5}
A - 6	1.22	-2.49×10^{-6}
A - 7	103.3	-6.76×10^{-4}
A - 8	29.70	-6.12×10^{-2}
A - 9	1.11	-1.29×10^{-4}
A - 12	26.50	-2.60×10^{-2}
A - 19	225.40	-4.14×10^{-4}
A - 20	28.80	-8.75×10^{-3}
B - 2	149.30	-5.58×10^{-3}
B - 3	18.40	-1.16×10^{-1}
B - 4	25.80	-3.93×10^{-3}
B - 5	3.00	-9.69×10^{-2}
2 - C	33.00	-1.51×10^{-1}
9 - C	6.40	-2.60×10^{-2}
Average	38.70	-3.04×10^{-2}
Stilling Well		
CW - 1	8.58	-1.12×10^{-1}
CW - 2	5.33	-2.86×10^{-2}
Average	6.96	7.00×10^{-2}

(b) North Fork Elk Creek	MMR	Recession Index (α)
Soil Well		
A - 1	2.02	-9.31×10^{-4}
A - 2	235	-2.69×10^{-1}
A - 3	47.60	-9.31×10^{-4}
A - 4	824	-9.93×10^{-3}
A - 5	3.64	-4.15×10^{-3}
A - 6	248.33	-1.75×10^{-2}
A - 8	11.71	-1.75×10^{-2}
B - 1	14.90	-1.37×10^{-3}
B - 3	1.81	-3.24×10^{-3}
B - 5	1.15	-1.32×10^{-3}
C - 1	10.33	-1.19×10^{-3}
C - 3	3.10	-2.31×10^{-4}
C - 5	3.13	-6.88×10^{-4}
Average	108.20	-2.52×10^{-2}
Stilling Well		
NFEC - 1	62.50	-3.53×10^{-1}
NFEC - 2	137.48	-2.53×10^{-1}
Average	99.99	-3.00×10^{-1}

Table 2. Generalized linear modelling coefficients and residual diagnostics, **(a)** probability of soil saturation and **(b)** scaled median water table height. Selected predictors, coefficients, null deviance, residual deviance and P-values are reported for each respective analysis. NA represents no value. Null represents analysis run only against mean of the response variable.

Response Variable	Predictor Variable	Coeff.	Null Deviance	Residual Deviance	P- value
(a) Proportion of saturation					
	Intercept	-13.98	59.26	NA	NA
	TWI	1.59	43.14	16.12	<.05
	Geology: NFEC	4.11	6.69	9.42	<.05
(b) Scaled median water table height					
	Intercept	3.46	100.54	NA	NA
	TWI	0.44	47.00	53.29	<.05
	Geology: NFEC	0.75	44.08	2.78	<.05
	Deficit	-.02	37.96	6.26	<.05

9.0 References

Amoozegar, A. (2001). Compact Constant Head Permeameter, users manual. *Ksat, Inc*.

Anderson, A. E., Weiler, M., Alila, Y., & Hudson, R. O. (2009). Subsurface flow velocities in a hillslope with lateral preferential flow. *Water Resources Research*, *45*(11).

Anderson, S.P, Dietrich, W.E., Montgomery, D.R.,Torres, R., Conrad, M.E, Loague, K., (1997). Subsurface Flow Paths in a Steep, Unchanneled Catchment. *Water Resources Research*, Vol. 33 (12), 2637–53. doi:10.1029/97WR02595.

Anderson, M. G., & Burt, T. P. (1978). The role of topography in controlling throughflow generation. *Earth Surface Processes and Landforms*, *3*(4), 331-344.

Appels, W.M., Graham, C.B., Freer, J. E., McDonnell, J.J., (2015). Factors affecting the spatial pattern of bedrock groundwater recharge at the hillslope scale. *Journal of Hydrology*, 29(21), 4594-4610.

Bachmair, S., & Weiler, M. (2011). New dimensions of hillslope hydrology. In *Forest hydrology and biogeochemistry* (pp. 455-481). Springer, Dordrecht.

Bergstrom, A., Jencso, K.J., Mcglynn, B.L., (2016). Spatiotemporal processes that contribute to hydrologic exchange between hillslopes, valley bottoms and streams. *Water Resources Research*, 52(6). Doi:10.1002/2015WR017972.

Beven, K. J., Kirkby, M.J., (1979). A Physically Based, Variable Contributing Area Model of Basin Hydrology. *Hydrological Sciences Bulletin* 24 (1): 43–69. doi:10.1080/02626667909491834.

Brenner, R. L., (1968). The Geology of Lubrecht Experimental Forest, University of Montana Library, 1-77.

Brown, V.A., McDonnell, J.J., Burns, D.A., Kendall, C., (1999). The Role of Event Water, a Rapid Shallow Flow Component, and Catchment Size in Summer Stormflow. *Journal of Hydrology* 217 (3-4): 171–90. doi:10.1016/S0022-1694(98)00247-9.

Burt, T. P., & Butcher, D. P. (1985). Topographic controls of soil moisture distributions. *European Journal of Soil Science*, *36*(3), 469-486.

Conrad, O., Bechtel, B., Bock, M., Dietrich, H., Fischer, E., Gerlitz, L., ... & Böhner, J. (2015). System for automated geoscientific analyses (SAGA) v. 2.1. 4. *Geoscientific Model Development*, *8*(7), 1991.

Covino, Timothy P., and Brian L. McGlynn. "Stream gains and losses across a mountain-to-valley transition: Impacts on watershed hydrology and stream water chemistry." *Water Resources Research* 43.10 (2007).

DeGagne, M. P., Douglas, G. G., Hudson, H. R., & Simonovic, S. P. (1996). A decision support system for the analysis and use of stage-discharge rating curves. *Journal of Hydrology*, *184*(3-4), 225-241.

Dobrowski, S. Z., Abatzoglou, J., Swanson, A. K., Greenberg, J. A., Mynsberge, A. R., Holden, Z. A., & Schwartz, M. K. (2013). The climate velocity of the contiguous United States during the 20th century. *Global Change Biology*, 19(1), 241–251.

Dobson, A. J., & Barnett, A. (2008). *An introduction to generalized linear models*. CRC press.

Dunne, T., Black, R.D., (1970). Partial Area Contributions to Storm Runoff in a Small New England Watershed. *Water Resources Research*, Vol. 6, No. 5.

Frisbee, M. D., Phillips, F. M., Weissmann, G. S., Brooks, P. D., Wilson, J. L., Campbell, A. R., & Liu, F. (2012). Unraveling the mysteries of the large watershed black box: Implications for the streamflow response to climate and landscape perturbations. *Geophysical Research Letters*, *39*(1).

Gabrielli, C.P., Mcdonnell, J.J., Jarvis, W.T., (2012). The Role of Bedrock Groundwater in Rainfall – Runoff Response at Hillslope and Catchment Scales. *Journal of Hydrology* 450-451. Elsevier B.V.: 117–33. doi:10.1016/j.jhydrol.2012.05.023.

Gardner, W. P., Susong, D. D., Solomon, D. K., & Heasler, H. (2010). Snowmelt hydrograph interpretation: Revealing watershed scale hydrologic characteristics of the Yellowstone volcanic plateau. *Journal of hydrology*, *383*(3-4), 209-222.

Graham, C.B., van Verseveld, W., Barnard, H.R., McDonnell, J.J., (2010). Estimating the deep seepage component of the hillslope and catchment water balance within a measurement uncertainty framework. *Hydrological Processes* 24 (25): 3631-3647.

Grayson, R.B., Western, A.A., Chiew, F.H.S., (1997). Preferred states in spatial soil moisture patterns: Local and nonlocal controls. *Water Resources Research*, Vol. 33, No. 12, 2897-2908.

Hale, V. C., & McDonnell, J. J. (2016). Effect of bedrock permeability on stream base flow mean transit time scaling relations: 1. A multiscale catchment intercomparison. *Water Resources Research*, *52*(2), 1358-1374.

Hale, V. C., McDonnell, J. J., Stewart, M. K., Solomon, D. K., Doolitte, J., Ice, G. G., & Pack, R. T. (2016). Effect of bedrock permeability on stream base flow mean transit time scaling relationships: 2. Process study of storage and release. *Water Resources Research*, *52*(2), 1375-1397.

Haria, A. H., & Shand, P. (2004). Evidence for deep sub-surface flow routing in forested upland Wales: implications for contaminant transport and stream flow generation. *Hydrology and Earth System Sciences Discussions*, *8*(3), 334-344.

Haught, D. R. W., & Meerveld, H. J. (2011). Spatial variation in transient water table responses: differences between an upper and lower hillslope zone. *Hydrological Processes*, *25*(25), 3866-3877.

Hopp, L., & McDonnell, J. J. (2009). Connectivity at the hillslope scale: Identifying interactions between storm size, bedrock permeability, slope angle and soil depth. *Journal of Hydrology*, *376*(3-4), 378-391.

Hoylman, Z. H., Jencso, K. G., Hu, J., Martin, J. T., Holden, Z. A., Seielstad, C. A., & Rowell, E. M. (2018). Hillslope topography mediates spatial patterns of ecosystem sensitivity to climate. *Journal of Geophysical Research: Biogeosciences*.

Hvorslev, M. J. (1951). Time lag and soil permeability in ground-water observations.

Jencso, K.G., McGlynn, B.L., Gooseff, M.N., Wondzell, S. M., Bencala, K. E., Marshall, L.A., (2009). Hydrologic Connectivity between Landscapes and Streams: Transferring Reach- and Plot-Scale Understanding to the Catchment Scale. *Water Resources Research*, 45 (4): 1–16. doi:10.1029/2008WR007225.

Jencso, K.G., McGlynn, B.L., Gooseff, M.N., Wondzell, S. M., Bencala, K. E., (2010). Hillslope hydrologic connectivity controls riparian groundwater turnover: Implications of catchment structure for riparian buffering and stream water sources. *Water Resources Research*, 46, W10524, doi:10.1029/2009WR008818

Jencso, K.G., McGlynn, B.L., (2011). Hierarchical controls on runoff generation : Topographically driven hydrologic connectivity, geology, and vegetation. *Water Resources Research* 47, W11527, doi: 10.1029/2011WR010666

Jiang, Q. (2003). Moist dynamics and orographic precipitation. *Tellus A*, *55*(4), 301-316.

Kendall, K. A., Shanley, J. B., & McDonnell, J. J. (1999). A hydrometric and geochemical approach to test the transmissivity feedback hypothesis during snowmelt. *Journal of Hydrology*, *219*(3-4), 188-205.

Kosugi, K. I., Katsura, S. Y., Katsuyama, M., & Mizuyama, T. (2006). Water flow processes in weathered granitic bedrock and their effects on runoff generation in a small headwater catchment. *Water Resources Research*, *42*(2).

Kosugi, K., Katsura, S., Mizuyama, T., Okunaka, S., Mizutani, T., (2008). Anomalous behavior of soil mantle groundwater demonstrates the major effects of bedrock groundwater on surface hydrological processes. *Water Resources Research*, Vol.44, W01407.

McDonnell, J. J. (1990). A rationale for old water discharge through macropores in a steep, humid catchment. *Water Resources Research*, *26*(11), 2821-2832.

McGlynn, B. L., & McDonnell, J. J. (2003). Quantifying the relative contributions of riparian and hillslope zones to catchment runoff. *Water Resources Research*, *39*(11).

Oliphant, A. J., Spronken-Smith, R. A., Sturman, A. P., & Owens, I. F. (2003). Spatial variability of surface radiation fluxes in mountainous terrain. *Journal of Applied Meteorology*, *42*(1), 113-128.

Pahl, P. J. (1981, June). Estimating the mean length of discontinuity traces. In *International Journal of Rock Mechanics and Mining Sciences & Geomechanics Abstracts*(Vol. 18, No. 3, pp. 221-228). Pergamon.

Penna, D., van Meerveld, H.J., Oliviero, O., Zuecco, G., Assendelft, R.S., Dalla Fontana, G., Borga, M., (2014). Seasonal changes in runoff generation in a small forested mountain catchment. *Hydrological Processes*, 29 2027-2042. doi: 10.1002/hyp.10347

Pfister, L., Martínez-Carreras, N., Hissler, C., Klaus, J., Carrer, G. E., Stewart, M. K., & McDonnell, J. J. (2017). Bedrock geology controls on catchment storage, mixing, and release: A comparative analysis of 16 nested catchments. *Hydrological processes*, *31*(10), 1828-1845.

Rempe, D. M., & Dietrich, W. E. (2014). A bottom-up control on fresh-bedrock topography under landscapes. *Proceedings of the National Academy of Sciences*, *111*(18), 6576-6581.

Rinderer, M., Van Meerveld, H. J., & Seibert, J. (2014). Topographic controls on shallow groundwater levels in a steep, prealpine catchment: When are the TWI assumptions valid?. *Water resources research*, *50*(7), 6067-6080.

Rowell, E., Seielstad, C., Goodburn, J., & Queen, L. (2009, October). Estimating plot-scale biomass in a western North American mixed-conifer forest from lidar-derived tree stems. In *Proc. SilviLaser Conf* (pp. 14-16).

Ruppel, E. T., & Lopez, D. A. (1984). *The thrust belt in southwest Montana and east-central Idaho*. US Government Printing Office.

Rupp, D. E., & Selker, J. S. (2006). On the use of the Boussinesq equation for interpreting recession hydrographs from sloping aquifers. *Water Resources Research*, *42*(12).

Schwartz, D.C., Zhang P.D.M. Fundamentals of Groundwater. (2003).

Seibert, J., Bishop, K., Rodhe, A., & McDonnell, J. J. (2003). Groundwater dynamics along a hillslope: A test of the steady state hypothesis. *Water Resources Research*, *39*(1).

Seibert, J., & McGlynn, B. L. (2007). A new triangular multiple flow direction algorithm for computing upslope areas from gridded digital elevation models. *Water resources research*, *43*(4).

Sidle, R. C., Noguchi, S., Tsuboyama, Y., & Laursen, K. (2001). A conceptual model of preferential flow systems in forested hillslopes: Evidence of self-organization. *Hydrological Processes*, *15*(10), 1675-1692.

Smith, R. S., Moore, R. D., Weiler, M., & Jost, G. (2014). Spatial controls on groundwater response dynamics in a snowmelt-dominated montane catchment. *Hydrology and Earth System Sciences*, *18*(5), 1835.

Sørensen, R., & Seibert, J. (2007). Effects of DEM resolution on the calculation of topographical indices: TWI and its components. *Journal of Hydrology*, *347*(1-2), 79-89.

Stephenson, N. (1998). Actual evapotranspiration and deficit: Biologically meaningful correlates of vegetation distribution across spatial scales. *Journal of Biogeography*, 25(5), 855–870.

Tague, C., & Grant, G. E. (2004). A geological framework for interpreting the low-flow regimes of Cascade streams, Willamette River Basin, Oregon. *Water Resources Research*, *40*(4).

Team, R. C. (2013). R: A language and environment for statistical computing.

Tromp-van Meerveld, H. J., & McDonnell, J. J. (2006). Threshold relations in subsurface stormflow: 1. A 147-storm analysis of the Panola hillslope. *Water Resources Research*, *42*(2).

Tromp-van Meerveld, H. J., & McDonnell, J. J. (2006). Threshold relations in subsurface stormflow: 2. The fill and spill hypothesis. *Water Resources Research*, *42*(2).

Tromp-van Meerveld, H. J., Peters, N. E., McDonnell, J. J., (2007). Effect of Bedrock Permeability on Subsurface Stormflow and the Water Balance of a Trenched Hillslope at the Panola Mountain Research Watershed, Georgia, USA. *Hydrological Processes* Vol. 21 (6), 750–69. doi:10.1002/hyp.6265.

U.S. Department of Agriculture, National Cooperative Soil Survey. (2001). Official Soil Series Descriptions: Lubrecht Series (Revision No. NRSCNG-JAL). Retrieved from https://soilseries.sc.egov.usda.gov/OSD_Docs/L/LUBRECHT.html

Viviroli, D., Weingartner, R., Messerli, B., (2003). Assessing the Hydrological Significance of the World's Mountains. *Mountain Research and Development*, Vol. 23, No1, 32-40.

Voeckler, H.M., Allen, D.A., Alila, Y., (2014). Modeling coupled surface water – Groundwater processes in a small mountainous headwater catchment. *Journal of Hydrology*, Vol. 517,1089–1106, http://dx.doi.org/10.1016/j.hydrol.2014.06.015

Uchida, T., Kosugi, K. I., & Mizuyama, T. (2002). Effects of pipe flow and bedrock groundwater on runoff generation in a steep headwater catchment in Ashiu, central Japan. *Water Resources Research*, *38*(7).

Uchida, T., Asano, Y., Ohte, N., Mizuyama, T. (2003). Seepage Area and Rate of Bedrock Groundwater Discharge at a Granitic Unchanneled Hillslope. *Water Resources Research*, Vol 38, 1–12, doi:10.1029/2002WR001298.\

Uchida, T., McDonnell, J. J., & Asano, Y. (2006). Functional intercomparison of hillslopes and small catchments by examining water source, flowpath and mean residence time. *Journal of Hydrology*, *327*(3-4), 627-642.

Watkins, H., Bond, C. E., Healy, D., & Butler, R. W. (2015). Appraisal of fracture sampling methods and a new workflow to characterise heterogeneous fracture networks at outcrop. *Journal of Structural Geology*, *72*, 67-82.

Weiler, M., McDonnell, J. J., Tromp-van Meerveld, I., & Uchida, T. (2005). Subsurface stormflow. *Encyclopedia of hydrological sciences*.

Western, A. W., Grayson, R. B., Blöschl, G., Willgoose, G. R., & McMahon, T. A. (1999). Observed spatial organization of soil moisture and its relation to terrain indices. *Water resources research*, *35*(3), 797-810.

Weyman, D. R. (1973). Measurements of the downslope flow of water in a soil. *Journal of Hydrology*, *20*(3), 267-288.

Whipkey, R. Z. (1965). Subsurface stormflow from forested slopes. *Hydrological Sciences Journal*, *10*(2), 74-85.

Wilson, J.L., Guan, H., (2004). Mountain-Block Hydrology and Mountain-Front Recharge.

Wilson, C. J., and W. E. Dietrich., (1987). The contribution of bedrock groundwater flow to storm runoff and high pore pressure development in hollows. *IAHS Publ*., 165, 49-59.

Winston, D., Link, P. K., Reed, J. C., Bickford, M. E., Houston, R. S., Rankin, D. W., ... & Van Schmus, W. R. (1993). Middle Proterozoic rocks of Montana, Idaho and eastern Washington: The Belt Supergroup. *Precambrian: Conterminous US*, *100*, 487-517.